JACS
JOURNAL OF THE AMERICAN CHEMICAL SOCIETY

Article

pubs.acs.org/JACS

# Supramolecular Scaffold for Tailoring the Two-Dimensional Assembly of Functional Molecular Units into Organic Thin Films

Franco King-Chi Leung,[†,‡,§] Fumitaka Ishiwari,[*,†,§] Takashi Kajitani,[†,§] Yoshiaki Shoji,[†,§] Takaaki Hikima,[§] Masaki Takata,[§,#] Akinori Saeki,[∥] Shu Seki,[⊥] Yoichi M. A. Yamada,[‡] and Takanori Fukushima[*,†]

[†]Laboratory for Chemistry and Life Science, Institute of Innovative Research, Tokyo Institute of Technology, 4259 Nagatsuta, Midori-ku, Yokohama 226-8503, Japan

[‡]RIKEN Center for Sustainable Resource Science, Wako, Saitama 351-0198, Japan

[§]RIKEN SPring-8 Center, 1-1-1 Kouto, Sayo, Hyogo 679-5148, Japan

[#]Institute of Multidisciplinary Research for Advanced Materials, Tohoku University, Sendai 980-8577, Japan

[∥]Department of Applied Chemistry, Graduate School of Engineering, Osaka University, 2-1 Yamadaoka, Suita, Osaka 565-0871, Japan

[⊥]Department of Molecular Engineering, Graduate School of Engineering, Kyoto University, Nishikyo-ku, Kyoto 615-8510, Japan

Supporting Information

**ABSTRACT:** Tailoring structurally anisotropic molecular assemblies while controlling their orientation on solid substrates is an important subject for advanced technologies that use organic thin films. Here we report a supramolecular scaffold based on tripodal triptycene assemblies, which enables functional molecular units to assemble into a highly oriented, multilayered two-dimensional (2D) structure on solid substrates. The triptycene building block carries an ethynyl group and three flexible side chains at the 10- and 1,8,13-positions, respectively. These bridgehead-substituted tripodal triptycenes self-assembled on solid substrates to form a well-defined "2D hexagonal + 1D lamellar" structure, which developed parallel to the surface of the substrates. Remarkably, the assembling properties of the triptycene building blocks, particularly for a derivative with tri(oxyethylene)-containing side chains, were not impaired when the alkyne terminal was functionalized with a large molecular unit such as $C_{60}$, which is comparable in diameter to the triptycene framework. Consequently, thin films with a multilayered 2D assembly of the $C_{60}$ unit were obtained. Flash-photolysis time-resolved microwave conductivity (FP-TRMC) measurements revealed that the $C_{60}$ film exhibits highly anisotropic charge-transport properties. Bridgehead-substituted tripodal triptycenes may provide a versatile supramolecular scaffold for tailoring the 2D assembly of molecular units into a highly oriented thin film, and in turn for exploiting the full potential of anisotropic molecular functions.

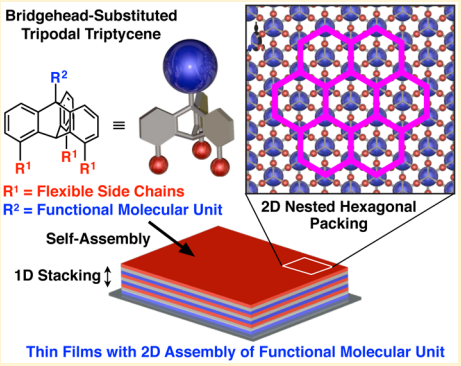


## INTRODUCTION

Thin films are practically important forms of materials for many applications. For organic thin films, the constituent molecules are usually anisotropic with respect to their structures and properties, and therefore, the precise control of the arrangement and orientation of the constituent molecules over a large area, ideally over the entire film, is desired to take full advantage of their inherent properties.[1−13] However, in reality, it is difficult to avoid the formation of multidomain structures, where each domain is randomly oriented with respect to the substrate surface. This is mainly due to the fact that molecular ordering occurs independently at multiple sites on substrates.

Recently, we reported a space-filling design for the rational synthesis of organic thin films with exceptionally long-range structural integrity.[14] This design strategy relies on the use of a particular type of tripodal triptycenes (Figure 1a), which self-assemble into a "2D hexagonal + 1D lamellar" structure through nested packing of the triple blades of the triptycene framework (Figure 1a). The nested hexagonal packing has been seen for some crystalline[15] and liquid crystalline[16] triptycene derivatives. On the basis of the geometrical requirement for tessellation, we demonstrated that the packing motif is eligible for achieving long-range propagation of 2D structural order.[14] For instance, a paraffinic derivative ($R^1 = OC_{12}H_{25}$) affords perfectly oriented macroscopic thin films on various substrates by simple vacuum evaporation or spin coating.[14] We envisioned that the "2D + 1D" structural motif of the tripodal triptycene assembly might serve as a supramolecular scaffold that could enable the controlled assembly of functional molecular units

**Received:** May 29, 2016
**Published:** August 22, 2016





DOI: 10.1021/jacs.6b05513
J. Am. Chem. Soc. 2016, 138, 11727−11733

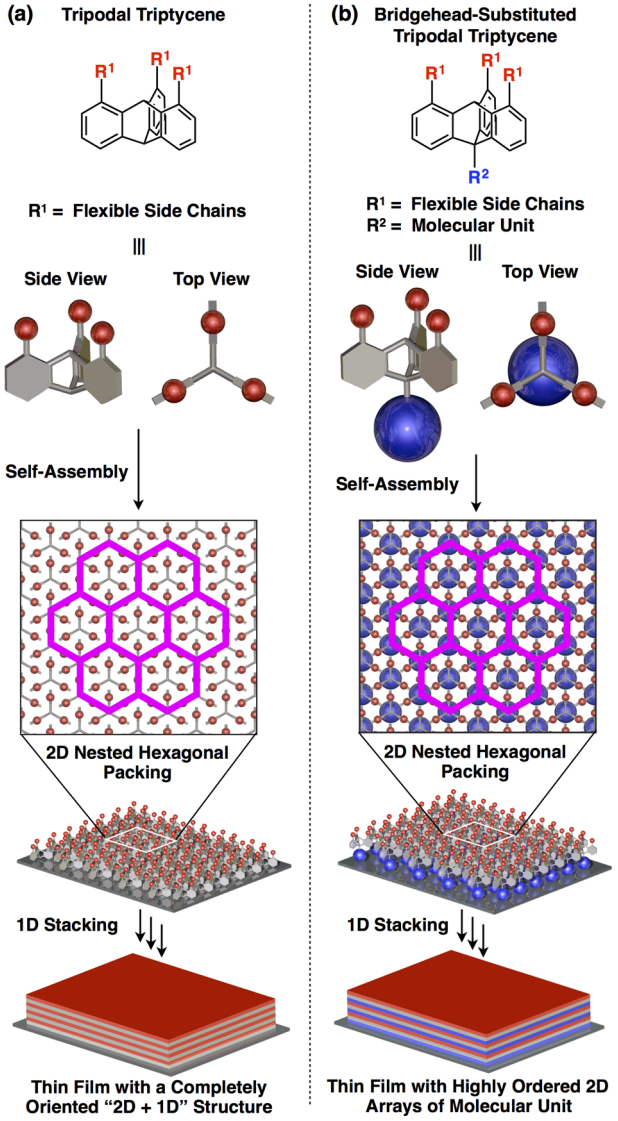


**Figure 1.** Schematic illustrations of the molecular structures of (a) tripodal triptycene and (b) bridgehead-substituted tripodal triptycene, and their assembled structures on a solid substrate.

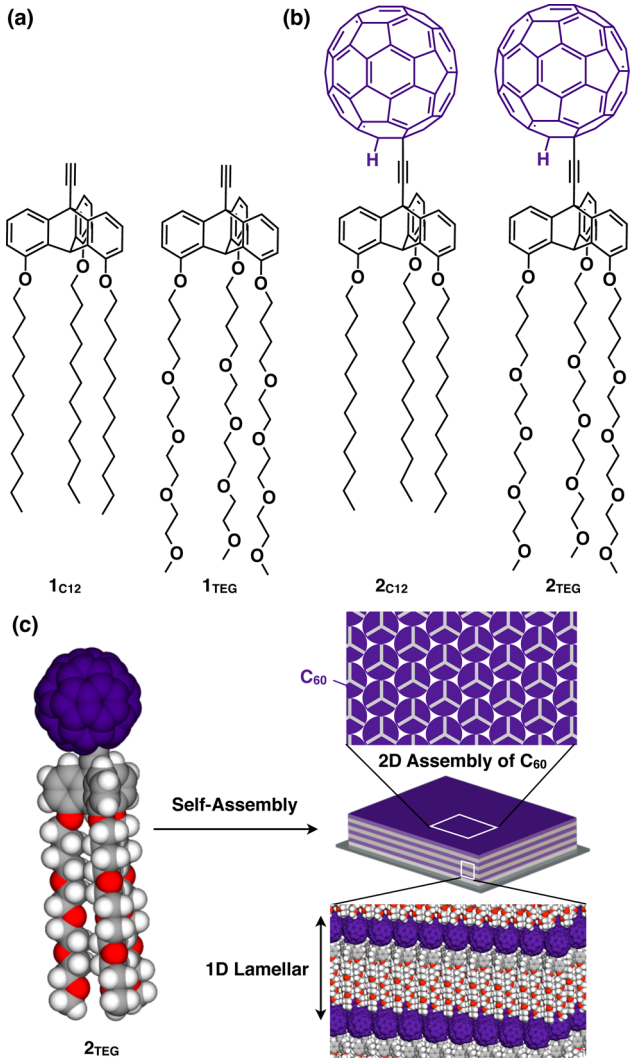


**Figure 2.** Chemical structures of (a) $\mathbf{1}_{C12}$ and $\mathbf{1}_{TEG}$, and (b) $\mathbf{2}_{C12}$ and $\mathbf{2}_{TEG}$. (c) Schematic illustration of the structure of a thin film formed from a $C_{60}$-appended tripodal triptycene, e.g., $\mathbf{2}_{TEG}$. The part of molecule ($C_{60}$ or side chain) that faces the substrate surface could not be determined.

into 2D arrays when the triptycene framework is properly modified.[14,17] Nevertheless, the incorporation of a bulky group into each aromatic ring (i.e., at the 4,5,16-positions) of the tripodal triptycene may impair the hexagonal nested packing. In this context, a bridgehead-substituted tripodal triptycene (Figure 1b) is interesting, since it may offer a sufficient space that can accommodate molecular units that are comparable in diameter to the triptycene framework.

Here we demonstrate that newly designed tripodal triptycenes ($\mathbf{1}_{C12}$ and $\mathbf{1}_{TEG}$, Figure 2a), carrying an ethynyl group and flexible side chains at the 10- (bridgehead) and 1,8,13-positions, respectively, can self-assemble on solid substrates to form a highly oriented thin film with a "2D + 1D" structure (Figure 1b), as reported for the prototype systems (Figure 1a).[14] Remarkably, even when the alkyne terminal is functionalized with a large $C_{60}$ unit, the resultant triptycene derivatives ($\mathbf{2}_{C12}$ and $\mathbf{2}_{TEG}$, Figure 2b) inherit the particular structuring capability of **1**, affording thin films with a highly oriented multilayered 2D assembly of $C_{60}$ (Figure 2c). This result reflects the utility of the tripodal triptycene assembly for the design of organic thin films with high structural anisotropy and orientational order (Figure 1b).

## RESULTS AND DISCUSSION

**Molecular Design and Synthesis.** The space-filling design using tripodal triptycenes is based on the nested 2D hexagonal packing of the triptycene blades. Moreover, long side chains attached to the triptycene framework endow the resultant assembly with flexibility to facilitate microphase separation as well as molecular reordering, leading to a thermodynamically favored structure. With the structural features of the triptycene building block in mind, we newly designed compounds $\mathbf{1}_{C12}$ and $\mathbf{1}_{TEG}$ (Figure 2a), where an ethynyl group was incorporated into the bridgehead position on the other side of the flexible side chains. The linear and rigid alkyne functionality is expected to allow the maximum use of the space around the triptycene framework. The terminal alkyne is also susceptible to chemical modifications and transformation. As flexible side chains, we used, along with a fully paraffinic dodecyl chain ($C_{12}H_{25}$), another side chain that contained triethylene glycol (TEG)


DOI: 10.1021/jacs.6b05513
J. Am. Chem. Soc. 2016, 138, 11727−11733

units to improve the solubility in common organic solvents. Furthermore, such long and polar side chains would enhance the microphase separation as well as softness of the assembled state.

1,8,10,13-Tetrasubstituted triptycene is a rare class of triptycene derivatives, and to the best of our knowledge the only reported example is the synthesis of 1,8,13-trichloro-10-alkyltriptycenes.[15c] Thus, we developed an efficient protocol for the synthesis of $\mathbf{1}_{C12}$ and $\mathbf{1}_{TEG}$ involving selective introduction of the corresponding functionalities into the framework of triptycene.[18] Scheme 1 outlines the synthesis of **1**. Bromination

**Scheme 1. Synthesis of 1 and 2**[a]

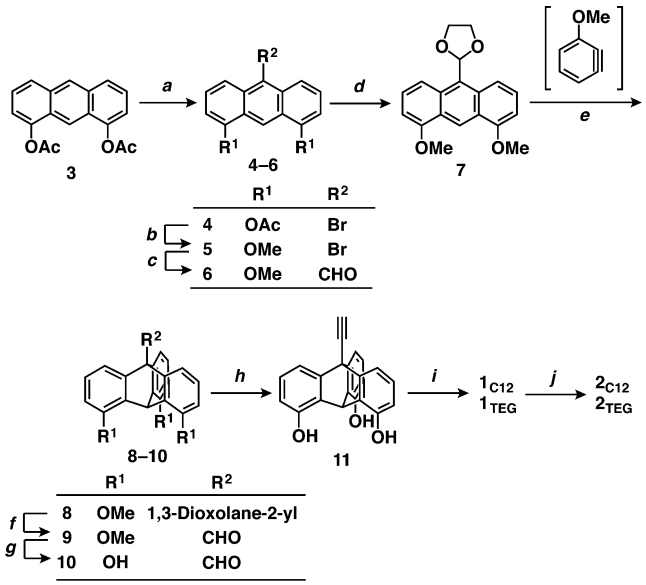


[a]Reagents and conditions: (a) NBS, DMF, 0 °C, 16 h → 25 °C, 2 h, 93%; (b) NaOH, $Me_2SO_4$, THF, 25 °C, 15 h, 70%; (c) *n*-BuLi, DMF, THF, −78 °C, 2 h, 92%; (d) ethylene glycol, TsOH, toluene, reflux, 48 h, 63%; (e) 2-methoxy-6-(trimethylsilyl)phenyl 1,1,1-trifluoromethane-sulfonate, CsF, MeCN, 65 °C, 18 h, 39%; (f) HCl, AcOH, 110 °C, 18 h, 95%; (g) $BBr_3$, $CH_2Cl_2$, 0 °C, 6 h, 90%; (h) 1-diazoacetonylphosphonic acid dimethyl ester (Ohira−Bestmann reagent), $K_2CO_3$, THF/MeOH, 25 °C, 5 h, 63%; (i) 1-bromododecane (for $\mathbf{1}_{C12}$ and $\mathbf{2}_{C12}$) or 15-bromo-2,5,8,11-tetraoxapentadecane (for $\mathbf{1}_{TEG}$ and $\mathbf{2}_{TEG}$), $K_2CO_3$, DMF, 75 °C, 18 h, 59% and 79% for $\mathbf{1}_{C12}$ and $\mathbf{1}_{TEG}$, respectively; (j) lithium bis(trimethylsilyl)-amide, $C_{60}$, THF, 25 °C, 2 h, HCl, 22% and 32% for $\mathbf{2}_{C12}$ and $\mathbf{2}_{TEG}$, respectively.

of 1,8-diacetoxyanthracene (**3**)[19] using NBS in DMF gave 1,8-diacetoxy-10-bromoanthracene (**4**)[20] in 93% yield. This bromination can be carried out using a relatively high-concentration solution of **3** (5.0 g/150 mL), which enables the gram-scale synthesis of **4**. Compound **4** was converted into **5** in 70% yield by alkaline hydrolysis, followed by methylation using $Me_2SO_4$. The bromo group of **5** was transformed into a formyl group through lithiation with *n*-BuLi in THF, followed by the reaction with DMF, to give **6** in 92% yield. The formyl group of **6** was converted into 1,3-dioxolane. Diels−Alder reaction of the resultant **7** with 3-methoxybenzyne, generated in situ from 2-methoxy-6-(trimethylsilyl)phenyl 1,1,1-trifluoromethanesulfonate, gave rise to triptycene derivative **8** in 39% yield. The presence of the dioxolane group leads to the formation of **8**, likely due to a steric effect as well as its weakly electron-donating properties. Note that Diels−Alder reaction of 3-methoxybenzyne and **6** with an electron-withdrawing formyl group resulted in a complex reaction mixture, in which the formation of the desired product (**9**) could not be detected. Deprotection of the dioxolane group of **8** with aqueous HCl in acetic acid resulted in **9** in 95% yield.[18] Single-crystal X-ray analysis confirmed the molecular structure of **9** (Figure S1). Similar to the case of previously reported 1,8,13-trimethoxytriptycene,[14] this compound in the crystal formed a pseudo hexagonal array through nested packing of the propeller-shaped triptycene blades. After demethylation of **9** by the reaction with $BBr_3$, the resultant **10** was treated with the Ohira−Bestmann reagent[21] in MeOH/THF to give **11** in 63% yield (two steps). Target compounds $\mathbf{1}_{C12}$ and $\mathbf{1}_{TEG}$ were obtained in 59 and 79% yields, respectively, by the Williamson reaction of **11** with the corresponding alkyl bromides in the presence of $K_2CO_3$ in DMF. The structures of all new compounds were unambiguously characterized by $^1H$, $^{13}C$ NMR, FT-IR spectroscopy, and high-resolution APCI-TOF mass spectrometry (Figures S16–S58).[18]

$C_{60}$-appended tripodal triptycenes $\mathbf{2}_{C12}$ and $\mathbf{2}_{TEG}$ (Figure 2b) were also designed to test the capacity of the new tripodal triptycene building blocks for the controlled 2D assembly of bulky molecular units. On the basis of molecular modeling, the diameter of $C_{60}$ (van der Waals diameter: 1.0 nm) and the cross-sectional area of triptycene (van der Waals diameter: 1.0 nm) are almost identical. Thus, $C_{60}$ appears to be the best motif for demonstrating the scope of the supramolecular scaffold. Besides, the controlled synthesis of $C_{60}$ assemblies have attracted considerable attention, because they potentially exhibit superb electronic properties for the development of organic electronic devices.[22,23]

Compound $\mathbf{2}_{C12}$ was obtained in 22% yield by the nucleophilic addition of in situ-generated lithium acetylide of $\mathbf{1}_{C12}$ to $C_{60}$ in THF.[18,24] The FAB mass spectrum of $\mathbf{2}_{C12}$ showed a clear ion peak of $m/z$ = 1550. 66 (calcd. for $C_{118}H_{86}O_3$ $[M]^+$: $m/z$ = 1550.66, Figure S54).[18] The $^1H$ NMR spectrum of $\mathbf{2}_{C12}$ in $CDCl_3$ at 25 °C displayed a singlet signal at 7.42 ppm arising from the proton attached to the $C_{60}$ unit, along with signals from aromatic and aliphatic protons of the triptycene and dodecyl side chains, respectively (Figure S51).[18] In the $^{13}C$ NMR spectrum of $\mathbf{2}_{C12}$, 30 signals due to the $C_{60}$ unit were detected, which is consistent with the symmetry of disubstituted $C_{60}$ (Figure S52).[18] With a procedure similar to that for $\mathbf{2}_{C12}$, compound $\mathbf{2}_{TEG}$ was obtained from $\mathbf{1}_{TEG}$ and $C_{60}$ in 32% yield and fully characterized by $^1H$ and $^{13}C$ NMR spectroscopy and FAB mass spectrometry (Figures S55–S58).[18]

**Self-Assembly Behaviors of Tripodal Triptycenes 1.** Tripodal triptycenes $\mathbf{1}_{C12}$ and $\mathbf{1}_{TEG}$ exhibited a phase behavior that involved only crystalline and isotropic liquid phases without the formation of any mesophase. For example, $\mathbf{1}_{C12}$ showed melting ($T_m$) and crystallization points ($T_c$) at 238 and 233 °C, respectively, in differential scanning calorimetry (DSC) (Figure S2a). The powder X-ray diffraction (XRD) pattern of a bulk sample of $\mathbf{1}_{C12}$ at 25 °C, observed upon cooling from its isotropic liquid in a glass capillary, displayed a diffraction pattern (Figures 3a,b and S3a), which is characteristic of the "2D hexagonal nested packing + 1D lamellar" structure of tripodal triptycenes.[14] The three XRD peaks with *d*-spacings of 2.51, 1.25, and 0.83 nm were indexed as diffractions from the (001), (002), and (003) planes, respectively, of a 1D lamellar structure. The observed layer spacing ($c$ = 2.50 nm) is comparable to the length of the longer molecular axis of $\mathbf{1}_{C12}$


DOI: 10.1021/jacs.6b05513
J. Am. Chem. Soc. 2016, 138, 11727−11733

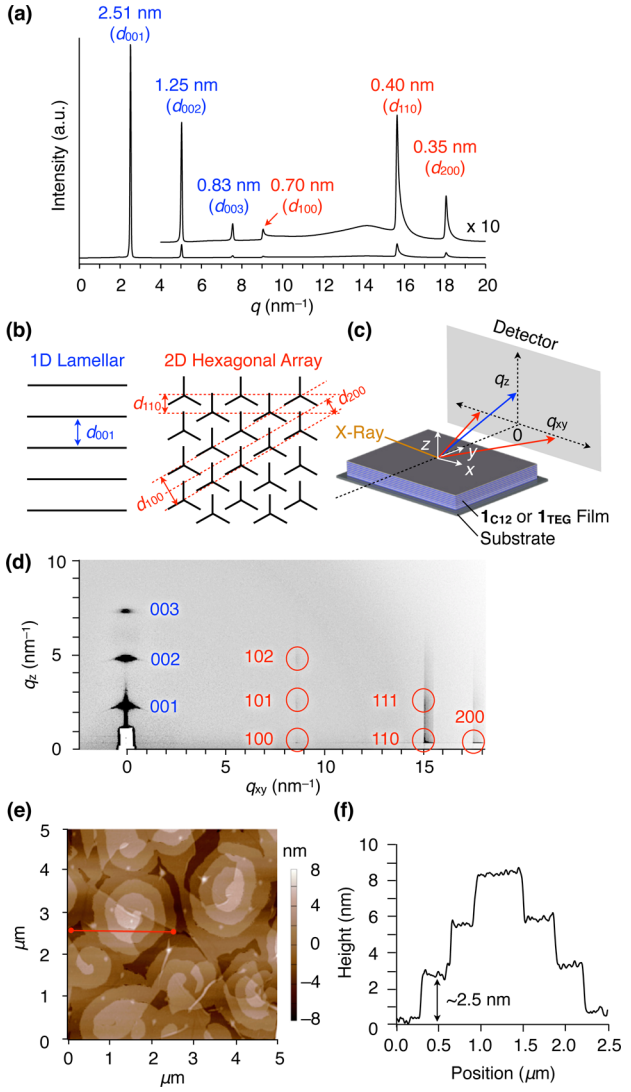


**Figure 3.** (a) Powder XRD pattern and its peak assignment of a bulk sample of $\mathbf{1}_{C12}$ at 25 °C on cooling from its isotropic liquid in a glass capillary (diameter: 1.5 mm). (b) Schematic illustration of the "2D + 1D" structure of self-assembled $\mathbf{1}_{C12}$. (c) Schematic illustration of the experimental setup for GI-XRD. (d) 2D GI-XRD image and Miller indices for the observed diffraction spots of a 50 nm-thick film of $\mathbf{1}_{C12}$, prepared by vacuum evaporation of $\mathbf{1}_{C12}$ onto a silicon wafer preheated at 120 °C. (e) AFM height image of a 50 nm-thick evaporated film of $\mathbf{1}_{C12}$, and (f) its height profile measured along the red line in (e).

(~2.6 nm). The XRD peaks observed in a wider-angle region ($q > 8$ nm$^{-1}$) have *d*-spacings of 0.70, 0.40, and 0.35 nm with a reciprocal ratio of 1:$\sqrt{3}$:2 and are thus assignable to diffractions from the (100), (110), and (200) planes of a 2D hexagonal lattice. The lattice parameter ($a$), defined as $2d_{100}/\sqrt{3}$, is 0.80 nm, which is comparable to those observed for previously reported tripodal triptycenes (0.81 nm).[14] Compound $\mathbf{1}_{TEG}$ showed a phase behavior similar to $\mathbf{1}_{C12}$. On the basis of DSC analysis (Figure S2b), the $T_m$ and $T_c$ of $\mathbf{1}_{TEG}$ were determined to be 189 and 185 °C, respectively. The powder XRD pattern of a bulk sample of $\mathbf{1}_{TEG}$ indicated the formation of 2D hexagonal nested packing and a 1D lamellar structure (Figure S3b). The hexagonal lattice parameter ($a$ = 0.82 nm) is identical to that of the assembly of $\mathbf{1}_{C12}$, and the layer spacing ($c$ = 2.74 nm) agrees with the length of the longer molecular axis of $\mathbf{1}_{TEG}$ (~2.7 nm).

Upon vacuum evaporation or spin coating, compounds $\mathbf{1}_{C12}$ and $\mathbf{1}_{TEG}$ successfully assembled on solid substrates to give a highly oriented thin film. For example, a thin film of $\mathbf{1}_{C12}$ with a thickness of 50 nm was obtained by vacuum evaporation onto a silicon wafer preheated at 120 °C. The 2D grazing-incidence XRD (GI-XRD) image of this film at 25 °C showed, in the meridional direction, intense spots with *d*-spacings of 2.61, 1.30, and 0.87 nm (Figures 3c,d and S4a). From the reciprocal *d*-spacing ratio, these spots were assigned to be diffractions from the (001), (002), and (003) planes, respectively, of a 1D lamellar structure, which developed parallel to the substrate. In the equatorial direction, three spots were observed with *d*-spacings of 0.72, 0.42, and 0.36 nm (Figures 3c,d and S4a), which correspond to diffractions from the (100), (110), and (200) planes of a hexagonal lattice, respectively. Thus, the nested packing of the triptycene unit of $\mathbf{1}_{C12}$ results in 2D hexagonal arrays, which pile up to form a layered structure parallel to the substrate. Consistent with this structural aspect of the thin film, the AFM image of the same film of $\mathbf{1}_{C12}$ showed an indented terrace structure (Figure 3e,f).[25] The height of each layer was approximately 2.5 nm, which is in good agreement with the layer spacing (2.61 nm) observed in the GI-XRD image. Similar to $\mathbf{1}_{C12}$, compound $\mathbf{1}_{TEG}$, upon vacuum evaporation, assembled on a silicon wafer to form a thin film with a "2D + 1D" structure. The comparison of the GI-XRD and AFM[25] data of the evaporated films of $\mathbf{1}_{C12}$ and $\mathbf{1}_{TEG}$ (Figure S4b–d) indicates that the structural and orientational orders of the "2D + 1D" assembly in their films are essentially identical.

In addition to the vacuum evaporation method, processing of a solution of $\mathbf{1}_{C12}$ and $\mathbf{1}_{TEG}$ using spin coating[18] also resulted in thin films that possess a "2D + 1D" structure with high orientational order. Accordingly, GI-XRD and AFM images of spin-coated films of $\mathbf{1}_{C12}$ and $\mathbf{1}_{TEG}$ on a silicon wafer, measured after thermal annealing at 120 °C for 1 h (Figures S5 and S6), were very similar to those observed for the evaporated films (Figures 3d,e and S4). Nevertheless, a closer look at the GI-XRD data showed that higher-order diffractions from the 1D layers as well as the diffractions from the hexagonal lattice are not explicit (Figures S5 and S6), indicating that the structural order of the "2D + 1D" assembly in the spin-coated films is relatively low compared to those in the evaporated films (Figures 3d and S4).

**Self-Assembly Behaviors of $C_{60}$-Appended Tripodal Triptycenes 2.** The bridgehead-substituted tripodal triptycenes underwent controlled assembly to form a "2D + 1D" structure even when covalently attached to $C_{60}$. However, $\mathbf{2}_{TEG}$ carrying TEG-containing side chains behaved much better than fully paraffinic $\mathbf{2}_{C12}$ in that a much higher order "2D + 1D" structure was achieved in the assembly of $\mathbf{2}_{TEG}$. This is most likely caused by the difference in the softness of the side chains: TEG-containing side chains may allow for molecular reorganization to correct small structural mismatches in the assembly.

$C_{60}$-appended $\mathbf{2}_{TEG}$ displayed no sign of phase transition in a temperature region from −50 to 250 °C (Figure S7a). Thermogravimetric analysis indicated that $\mathbf{2}_{TEG}$ has a high thermal stability (thermolysis onset temperature = 390 °C, Figure S8a). The powder XRD pattern of a bulk sample of $\mathbf{2}_{TEG}$ in a glass capillary at 25 °C showed broad diffraction peaks (Figures 4a and S9a). A clear XRD peak with a *d*-spacing of 5.02 nm was indexed as diffraction from the (001′) plane of a 1D lamellar structure. If we consider both the layer spacing ($c$ =


DOI: 10.1021/jacs.6b05513
J. Am. Chem. Soc. 2016, 138, 11727−11733

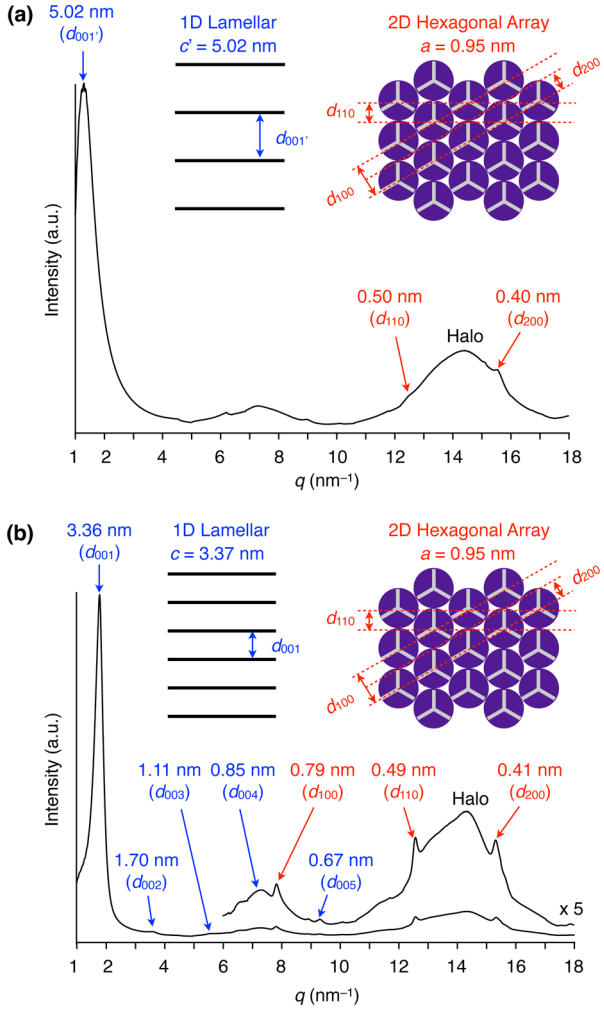


**Figure 4.** Powder XRD patterns and their peak assignments of a bulk sample of $\mathbf{2}_{TEG}$ (a) before and (b) after thermal annealing at 120 °C for 1 h in a glass capillary (diameter: 1.5 mm). Insets represent schematic illustrations of the structural elements and parameters of self-assembled $\mathbf{2}_{TEG}$ before and after thermal annealing.

5.02 nm) and the length of the longer molecular axis of $\mathbf{2}_{TEG}$ (~3.4 nm), a bilayer lamellar structure, rather than a monolayer lamellar structure, likely forms (Figure 4a, inset). Meanwhile, the XRD peaks with *d*-spacings of 0.50 and 0.40 nm can be assigned as diffractions from the (110) and (200) planes of the hexagonal lattice with $a$ = 0.95 nm (Figure 4a, inset). This value is larger than that of the 2D hexagonal lattice formed in the assembly of $\mathbf{1}_{TEG}$ ($a$ = 0.82 nm), but is comparable to the diameter of $C_{60}$ (1.0 nm). Thus, a periodic hexagonal assembly of the $C_{60}$ units, brought about by the triptycene scaffold, is mainly responsible for the diffractions.

Notably, thermal annealing resulted in a dramatic change in the assembly structure of $\mathbf{2}_{TEG}$. The XRD pattern of $\mathbf{2}_{TEG}$ at 25 °C, observed after thermal annealing at 120 °C for 1 h, showed five XRD peaks with *d*-spacings of 3.36, 1.70, 1.11, 0.85, and 0.67 nm (Figure 4b), which are indexed as diffractions from the (001), (002), (003), (004), and (005) planes of the 1D lamellar, respectively (Figure S9b). The layer spacing significantly decreased from 5.02 to 3.37 nm (Figure 4), which agrees with the length of the longer molecular axis of $\mathbf{2}_{TEG}$ (~3.4 nm). This change can be rationally explained by considering that transformation from the bilayer lamellar to a monolayer lamellar structure occurs upon thermal annealing. Furthermore, the 2D hexagonal structural order was greatly improved by the thermal treatment. Accordingly, three XRD peaks with *d*-spacings of 0.79, 0.49, and 0.41 nm were clearly observed (Figure 4b). From their reciprocal *d*-spacing ratio (1:$\sqrt{3}$:2), these peaks were unambiguously characterized as diffractions from the (100), (110), and (200) planes of the hexagonal lattice with $a$ = 0.95 nm (Figure S9b).

Fully paraffinic $\mathbf{2}_{C12}$ also self-assembled to form a "2D hexagonal packing and 1D bilayer" structure ($a$ = 0.97 nm and $c$ = 5.22 nm, Figure S10a). However, the powder XRD pattern of a bulk sample of $\mathbf{2}_{C12}$ (Figure S10a) was broader than that observed for the bulk sample of $\mathbf{2}_{TEG}$ (Figure 4). Even after thermal annealing at 120 °C for 1 h,[27] it remained almost unchanged, except that a very small peak with a *d*-spacing of 3.24 nm newly arose from a monolayer lamellar structure (Figure S10b). In contrast to the case of $\mathbf{2}_{TEG}$, transformation of the assembly of $\mathbf{2}_{C12}$ into a higher order structure is largely suppressed, and thus the bilayer lamellar structure, which may be kinetically favored, prevails over a thermodynamically favored monolayer lamellar structure.

**Thin Films with Highly Oriented 2D Hexagonal Arrays of $C_{60}$ Units Using the Tripodal Triptycene Building Blocks.** We prepared a thin film of $\mathbf{2}_{TEG}$ by simply spin coating (500 rpm) a toluene solution of $\mathbf{2}_{TEG}$ (1.0 mmol/L) on a silicon wafer, followed by thermal annealing at 120 °C for 1 h. The GI-XRD image of this film at 25 °C showed, in the meridional direction, clear diffraction spots (Figures 5 and S11), which were characterized as diffractions from the (001), (002), (003), (004), and (006) planes of a monolayer lamellar structure with a layer spacing of 3.31 nm. In the equatorial direction, three short arcs arising from diffractions from the (100), (110), and (200) planes of a 2D hexagonal lattice ($a$ = 0.97 nm) were observed. These observations allowed us to conclude that $C_{60}$-appended $\mathbf{2}_{TEG}$ is capable of forming a highly oriented thin film, where the multilayers of the 2D hexagonal $C_{60}$ arrays develop parallel to the substrate surface (Figure 5a). To further confirm the orientational order of the assembly of $\mathbf{2}_{TEG}$ on substrates, we measured a through-view XRD image using a relatively thick film. To prepare the film sample, a toluene solution of $\mathbf{2}_{TEG}$ (1.0 mmol/L) was sandwiched between two sapphire substrates, and then the solvent was slowly evaporated under ambient conditions. Figure S12 shows the through-view XRD image of the resultant film. Notably, only diffraction spots from the (100), (110), and (200) planes of the hexagonal lattice were observed without any diffractions from the (00*l*) planes of the lamellar structures (Figure S12). This result strongly supports the above conclusion regarding the orientational order of the "2D + 1D" structure of $\mathbf{2}_{TEG}$ on the substrates. Therefore, the tripodal triptycene scaffold enables the formation of thin films with 2D assembly of the $C_{60}$ unit, which are perfectly oriented parallel to the substrate surface.

As described in the previous section, $\mathbf{2}_{C12}$ in the bulk formed a less ordered assembly than $\mathbf{2}_{TEG}$. Likewise, a spin-coated film of $\mathbf{2}_{C12}$, obtained under conditions identical to those for $\mathbf{2}_{TEG}$, had relatively low quality in terms of the structural and orientational order of the "2D + 1D" assembly, and only an X-ray diffraction due to the 1D monolayer lamellar was observed in its GI-XRD image (Figure S13). Furthermore, the surface roughness of the film of $\mathbf{2}_{C12}$ (root-mean-square surface roughness = 1.08 nm, Figure S14b) was more than three times higher than that of the film of $\mathbf{2}_{TEG}$ (root-mean-square


DOI: 10.1021/jacs.6b05513
J. Am. Chem. Soc. 2016, 138, 11727−11733

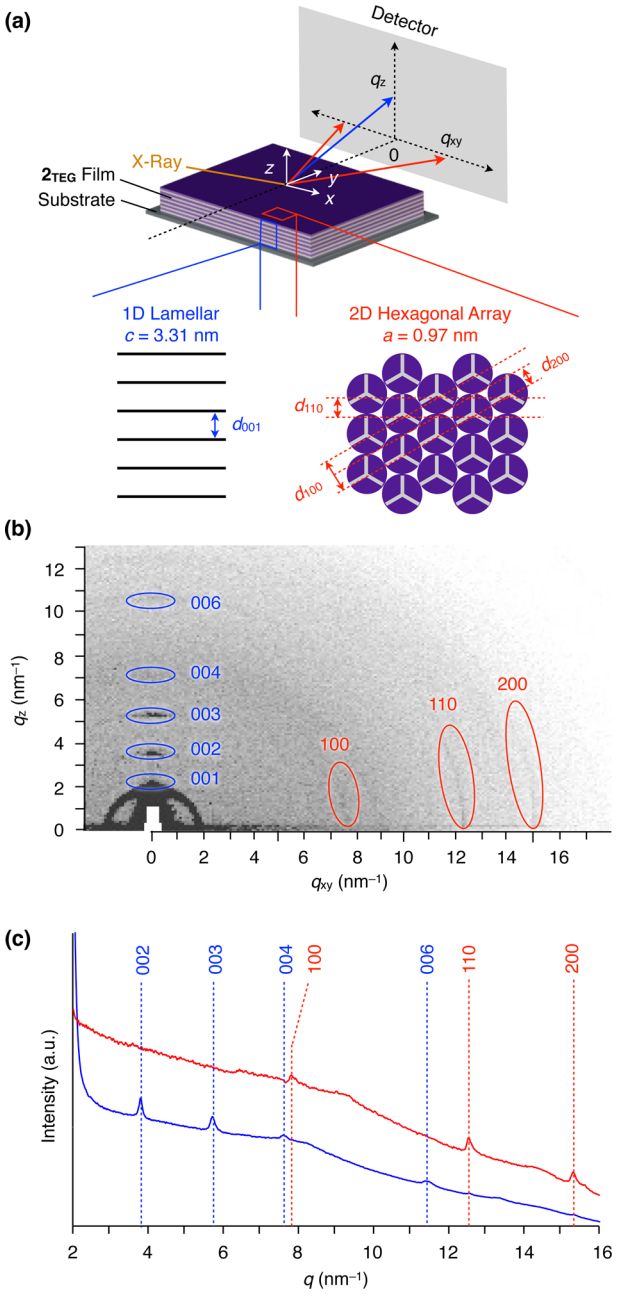


**Figure 5.** (a) Schematic illustration of the experimental setup for 2D GI-XRD, along with the structure of a spin-coated film of $\mathbf{2}_{TEG}$ on a silicon wafer. (b) 2D GI-XRD image and (c) its 1D-XRD profile (blue: meridional direction, red: equatorial direction) of the spin-coated film of $\mathbf{2}_{TEG}$, measured after thermal annealing (120 °C, 1 h).

surface roughness = 0.30 nm, Figure S14a). Obviously, the controlled assembly of a bulky and rigid group such as $C_{60}$ using the triptycene scaffold should require sufficiently soft side chains that allow molecular reordering.

**Conducting Properties of the Thin Film with Highly Oriented 2D Hexagonal Arrays of $C_{60}$ Units.** Since the thin film of $\mathbf{2}_{TEG}$ possesses a highly oriented, multilayered 2D assembly of $C_{60}$ (Figure 2c), the charge-transport properties of the film along the direction parallel to the substrate surface should be better than those in the perpendicular direction (Figure 6a). To confirm the anisotropic conducting behavior expected from the structural feature of the film (Figure 6a), we carried out flash-photolysis time-resolved microwave conductivity (FP-TRMC) measurements using a thin film of $\mathbf{2}_{TEG}$, which was sandwiched between quartz substrates and thermally annealed at 120 °C for 1 h. This method makes it possible to evaluate the intrinsic charge-transport properties of materials as well as anisotropy without attaching electrodes.[28] Thus, the sandwiched film of $\mathbf{2}_{TEG}$ was placed in a microwave resonant cavity in such a way that the electric-field vector of the microwave could be polarized in a direction parallel or perpendicular to the substrate surface and then exposed to a laser-pulse (wavelength = 266 nm) with a photon density of 6.8 × $10^{15}$ photons cm$^{-2}$. Figure 6b shows the resultant rise and decay profiles of transient conductivities parallel (red) and perpendicular (blue) to the substrate. Here, the transient conductivity is defined as $\phi\Sigma\mu$, where $\phi$ and $\Sigma\mu$ are the photocarrier-generation yield and the sum of the mobilities of the generated charge carriers, respectively. Analysis of profiles gave the maximum transient conductivities in the parallel ($\phi\Sigma\mu_{para}$ = 1.0 × $10^{-2}$ cm$^2$/V s) and perpendicular ($\phi\Sigma\mu_{perp}$ = 1.9 × $10^{-3}$ cm$^2$/V s) directions, which in turn gave a degree of anisotropy ($\phi\Sigma\mu_{para}/\phi\Sigma\mu_{perp}$) of 5.3.[29] This result, which is obviously brought about by the structural anisotropy of the film, may be interesting in that spherical $C_{60}$ has no inherent preference for 2D assembly and exhibit large anisotropic conduction.

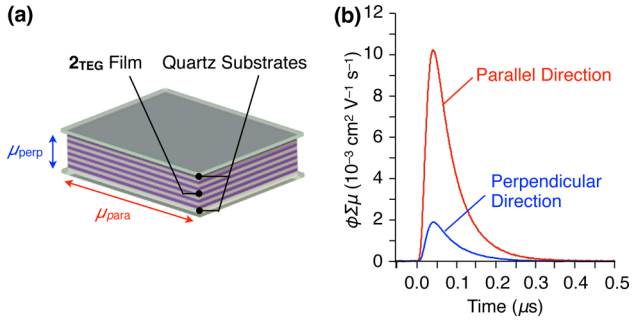


**Figure 6.** (a) Schematic illustration of a thin film of $\mathbf{2}_{TEG}$ sandwiched between quartz plates for FP-TRMC measurements. (b) FP-TRMC profiles of the thin film of $\mathbf{2}_{TEG}$ at 25 °C, observed along parallel (red) and perpendicular (blue) directions to the substrate surface.

## CONCLUSIONS

Inspired by the remarkable self-assembling properties of paraffinic tripodal triptycenes that lead to the spontaneous formation of thin films with a completely oriented "2D + 1D" structure (Figure 1a),[14] we have developed a supramolecular scaffold for tailoring the 2D assembly of functional molecular units into organic thin films (Figure 1b). The building block of the supramolecular scaffold consists of newly designed tripodal triptycene (**1**, Figure 2a), which has a terminal alkyne unit at the bridgehead position for covalent modifications. This design enables the use of molecular units with a diameter as large as approximately 1 nm for controlled 2D assembly. We chose $C_{60}$ to demonstrate the assembling ability of the supramolecular scaffold. We found that the $C_{60}$-appended tripodal triptycene thus synthesized (**2**, Figure 2b), when carrying very flexible side chains to allow reordering of the resulting assembly, gives a thin film with a highly ordered and orientated "2D + 1D" structure on solid substrates, where the $C_{60}$ units are densely clustered two dimensionally. Consequently, this thin film exhibited anisotropic conducting properties. Considering that triptycene-based supramolecular scaffolds are capable of directing functional molecular units to assemble into a highly oriented



DOI: 10.1021/jacs.6b05513
J. Am. Chem. Soc. 2016, 138, 11727−11733

anisotropic 2D structure that is compatible with the geometry of substrate surfaces, the present approach may contribute to the design of high-performance organic thin films with anisotropic functionalities.

## ■ ASSOCIATED CONTENT

### Supporting Information

The Supporting Information is available free of charge on the ACS Publications website at DOI: 10.1021/jacs.6b05513.

Synthesis, $^{1}H$ and $^{13}C$ NMR spectra, FT-IR spectra, high-resolution MS spectra, DSC and TGA profiles, powder XRD profiles, GI-XRD images, AFM images, FP-TRMC profile (PDF)

Crystallographic data for **9** (CIF)

## ■ AUTHOR INFORMATION


### Corresponding Authors

*ishiwari@res.titech.ac.jp

*fukushima@res.titech.ac.jp


### Notes

The authors declare no competing financial interest.

## ■ ACKNOWLEDGMENTS

This work was supported by a Grant-in-Aid for Scientific Research on Innovative Areas "π-Figuration" (no. 26102008) of The Ministry of Education, Culture, Sports, Science, and Technology, Japan. The synchrotron XRD experiments were performed at BL45XU in SPring-8 with the approval of the RIKEN SPring-8 Center (20140056 and 20150068). The authors thank Yuki Kida for his assistance in the synthesis of compound **11**. F.K.C.L acknowledges the International Program Associate (IPA) of RIKEN.

## ■ REFERENCES


(1) Dimitrakopoulos, C. D.; Malenfant, P. R. L. *Adv. Mater.* **2002**, *14*, 99−117.

(2) Wu, J.; Pisula, W.; Müllen, K. *Chem. Rev.* **2007**, *107*, 718−747.

(3) Murphy, A. R.; Fréchet, J. M. J. *Chem. Rev.* **2007**, *107*, 1066−1096.

(4) Wang, C.; Dong, H.; Hu, W.; Liu, Y.; Zhu, D. *Chem. Rev.* **2012**, *112*, 2208−2267.

(5) Mei, J.; Diao, Y.; Appleton, A. L.; Fang, L.; Bao, Z. *J. Am. Chem. Soc.* **2013**, *135*, 6724−6746.

(6) Takimiya, K.; Osaka, I.; Mori, T.; Nakano, M. *Acc. Chem. Res.* **2014**, *47*, 1493−1502.

(7) Hasegawa, T.; Takeya, J. *Sci. Technol. Adv. Mater.* **2009**, *10*, 024314.

(8) Shekhah, O.; Liu, J.; Fischerb, R. A.; Wöll, Ch. *Chem. Soc. Rev.* **2011**, *40*, 1081−1106.

(9) Colson, J. W.; Dichtel, W. R. *Nat. Chem.* **2013**, *5*, 453−465.

(10) Wu, G.; Zhang, X. *Polymer Thin Films* **2010**, *9*, 143−160.

(11) Ariga, K.; Yamauchi, Y.; Mori, T.; Hill, J. P. *Adv. Mater.* **2013**, *25*, 6477−6512.

(12) Hosono, N.; Kajitani, T.; Fukushima, T.; Ito, K.; Sasaki, S.; Takata, M.; Aida, T. *Science* **2010**, *330*, 808−811.

(13) Osawa, T.; Kajitani, T.; Hashizume, D.; Ohsumi, H.; Sasaki, S.; Takata, M.; Koizumi, Y.; Saeki, A.; Seki, S.; Fukushima, T.; Aida, T. *Angew. Chem., Int. Ed.* **2012**, *51*, 7990−7993.

(14) Seiki, N.; Shoji, Y.; Kajitani, T.; Ishiwari, F.; Kosaka, A.; Hikima, T.; Takata, M.; Someya, T.; Fukushima, T. *Science* **2015**, *348*, 1122−1126.

(15) (a) Ardebili, M. H. P.; Dougherty, D. A.; Mislow, K.; Schwartz, L. H.; White, J. G. *J. Am. Chem. Soc.* **1978**, *100*, 7994−7997. (b) Yamamura, K.; Kawashima, T.; Eda, K.; Tajima, F.; Hashimoto, M. *J. Mol. Struct.* **2005**, *737*, 1−6. (c) Chmiel, J.; Heesemann, I.; Mix, A.; Neumann, B.; Stammler, H. G.; Mitzel, N. W. *Eur. J. Org. Chem.* **2010**, *2010*, 3897−3907.

(16) (a) Norvez, S.; Simon, J. *J. Chem. Soc., Chem. Commun.* **1990**, *26*, 1398−1399. (b) Norvez, S. *J. Org. Chem.* **1993**, *58*, 2414−2418.

(17) Shioya, H.; Shoji, Y.; Seiki, N.; Nakano, M.; Fukushima, T.; Iwasa, Y. *Appl. Phys. Express* **2015**, *8*, 121101−121104.

(18) See the Supporting Information.

(19) Brockmann, H.; Budde, G. *Chem. Ber.* **1952**, *86*, 432−433.

(20) Davis, N. K. S.; Pawlicki, M.; Anderson, H. L. *Org. Lett.* **2008**, *10*, 3945−3947.

(21) (a) Ohira, S. *Synth. Commun.* **1989**, *19*, 516−564. (b) Müller, S.; Liepold, B.; Roth, G. J.; Bestmann, H. J. *Synlett* **1996**, *6*, 521−522.

(22) (a) Segura, J. L.; Martín, N.; Guldi, D. M. *Chem. Soc. Rev.* **2005**, *34*, 31−47. (b) Muñoz, A.; Illescas, B. M.; Sánchez-Navarro, M.; Rojo, J.; Martín, N. *J. Am. Chem. Soc.* **2011**, *133*, 16758−16761. (c) Vergara, J.; Barberá, J.; Serrano, J. L.; Ros, M. B.; Sebastián, N.; de la Fuente, M. R.; López, D. O.; Fernández, G.; Sánchez, L.; Martín, N. *Angew. Chem., Int. Ed.* **2011**, *50*, 12523−12528. (d) Nakanishi, T.; Shen, Y.; Wang, J.; Yagai, S.; Funahashi, M.; Kato, T.; Fernandes, P.; Mohwald, H.; Kurth, D. G. *J. Am. Chem. Soc.* **2008**, *130*, 9236−9237. (e) Li, W.-S.; Yamamoto, Y.; Fukushima, T.; Saeki, A.; Seki, S.; Tagawa, S.; Masunaga, H.; Sasaki, S.; Takata, M.; Aida, T. *J. Am. Chem. Soc.* **2008**, *130*, 8886−8887. (f) Wang, J.; Shen, Y.; Kessel, S.; Fernandes, P.; Yoshida, K.; Yagai, S.; Kurth, D. G.; Moehwald, H.; Nakanishi, T. *Angew. Chem., Int. Ed.* **2009**, *48*, 2166−2170. (g) Zhong, Y.-W.; Matsuo, Y.; Nakamura, E. *J. Am. Chem. Soc.* **2007**, *129*, 3052−3053. (h) Li, C.-Z.; Matsuo, Y.; Nakamura, E. *J. Am. Chem. Soc.* **2009**, *131*, 17058−17059. (i) Zhang, X.; Hsu, C.-H.; Ren, X.; Gu, Y.; Song, B.; Sun, H.-J.; Yang, S.; Chen, E.; Tu, Y.; Li, X.; Yang, X.; Li, Y.; Zhu, X. *Angew. Chem., Int. Ed.* **2015**, *54*, 114−117. (j) Chikamatsu, M.; Nagamatsu, S.; Yoshida, Y.; Saito, K.; Yase, K.; Kikuchi, K. *Appl. Phys. Lett.* **2005**, *87*, 203504. (k) Choi, B.; Yu, J.; Paley, D. W.; Trinh, M. T.; Paley, M. V.; Karch, J. M.; Crowther, A. C.; Lee, C.-H.; Lalancette, R. A.; Zhu, X.; Kim, P.; Steigerwald, M. L.; Nuckolls, C.; Roy, X. *Nano Lett.* **2016**, *16*, 1445−1449.

(23) (a) Kira, A.; Umeyama, T.; Matano, Y.; Yoshida, K.; Isoda, S.; Park, J. K.; Kim, D.; Imahori, H. *J. Am. Chem. Soc.* **2009**, *131*, 3198−3200. (b) Novak, M.; Ebel, A.; Meyer-Friedrichsen, T.; Jedaa, A.; Vieweg, B. F.; Yang, G.; Voitchovsky, K.; Stellacci, F.; Spiecker, E.; Hirsch, A.; Halik, M. *Nano Lett.* **2011**, *11*, 156−159. (c) Jäger, C. M.; Schmaltz, T.; Novak, M.; Khassanov, A.; Vorobiev, A.; Hennemann, M.; Krause, A.; Dietrich, H.; Zahn, D.; Hirsch, A.; Halik, M.; Clark, T. *J. Am. Chem. Soc.* **2013**, *135*, 4893−4900. (d) Lacher, S.; Matsuo, Y.; Nakamura, E. *J. Am. Chem. Soc.* **2011**, *133*, 16997−17004. (e) Hayashi, H.; Sobczuk, A.; Bolag, A.; Sakai, N.; Matile, S. *Chem. Sci.* **2014**, *5*, 4610−4614.

(24) (a) Shirai, Y.; Osgood, A. J.; Zhao, Y. M.; Kelly, K. F.; Tour, J. M. *Nano Lett.* **2005**, *5*, 2330−2334. (b) Shirai, Y.; Osgood, A. J.; Zhao, Y.; Yao, Y.; Saudan, L.; Yang, H.; Yu-Huang, C.; Alemany, L. B.; Sasaki, T.; Morin, J.-F.; Guererro, J. M.; Kelly, K. F.; Tour, J. M. *J. Am. Chem. Soc.* **2006**, *128*, 4854−4864.

(25) The AFM image is reminiscent of those observed for the systems that involve screw dislocation during crystallization.[26]

(26) (a) Chow, E. H. H.; Bučara, D.-K.; Jones, W. *Chem. Commun.* **2012**, *48*, 9210−9226. (b) Cuppen, H. M.; Graswinckel, W. S.; Meekes, H. *Cryst. Growth Des.* **2004**, *4*, 1351−1357.

(27) The DSC and TGA analysis of $\mathbf{2}_{C12}$ did not show any signs of a phase transition or decomposition at temperatures ranging from −50 to 250 °C (Figures S7b and S8b).

(28) (a) Seki, S.; Saeki, A.; Sakurai, T.; Sakamaki, D. *Phys. Chem. Chem. Phys.* **2014**, *16*, 11093−11113. (b) Saeki, A.; Seki, S.; Takenobu, T.; Iwasa, Y.; Tagawa, S. *Adv. Mater.* **2008**, *20*, 920−923. (c) Amaya, T.; Seki, S.; Moriuchi, T.; Nakamoto, K.; Nakata, T.; Sakane, H.; Saeki, A.; Tagawa, S.; Hirao, T. *J. Am. Chem. Soc.* **2009**, *131*, 408−409.

(29) As shown in Figure S15, the FP-TRMC signals of an as-cast film of $\mathbf{2}_{TEG}$ without thermal annealing were rather weak in both parallel and perpendicular directions, and the degree of anisotropy was 1.3.